INSTITUTE OF PHYSICS PUBLISHING JOURNAL OF PHYSICS: CONDENSED MATTER

J. Phys.: Condens. Matter **14** (2002) 3333–3352 PII: S0953-8984(02)31066-X

Infrared spectra of Si–O overtones, hydrous species, and U ions in metamict zircon: radiation damage and recrystallization

Ming Zhang[1,3], **Ekhard K H Salje**[1] **and Rodney C Ewing**[2]

[1] Department of Earth Sciences, University of Cambridge, Downing Street, Cambridge CB2 3EQ, UK
[2] Department of Nuclear Engineering and Radiological Sciences, Department of Geological Sciences, University of Michigan, Ann Arbor, MI 48109-2104, USA

E-mail: mz10001@esc.cam.ac.uk

Received 21 November 2001
Published 15 March 2002
Online at stacks.iop.org/JPhysCM/14/3333

Abstract

Radiation damage and recrystallization in natural zircons have been studied by analysing Si–O stretching overtones/combinations, hydrous species, and U-ion spectra in the frequency region between 1200 and 11 000 cm^{-1}. The effects of radiation are characterized by a dramatic variation of intensity, a decrease in frequencies of multi-phonon bands (e.g., Si–O stretching overtones), a change of spectral profile of OH species, a formation of new OH species, and new signals related to U ions. The formation of new anisotropic OH species in the crystalline regions of metamict zircon is observed and this could account for the different thermal behaviour of OH species between metamict zircon and titanite during high-temperature annealing. The results imply systematic modifications of the local environments of the OH and U ions in the damage process. Both U^{4+} and U^{5+} spectra show dramatic variations during metamictization. We observe, for the first time, that as a result of radiation damage, the U^{5+} signals near 6668 and 9030 cm^{-1} become undetectable at a dose of around 1.5×10^{18} α-events g^{-1} while extra lines near 6650 and 8969 cm^{-1} appear. These variations are interpreted as radiation-induced local modifications in crystalline regions. The general shape of the U-ion spectrum of the crystalline zircon is somehow still preserved in highly damaged zircon. A decomposed zircon, consisting of ZrO_2, SiO_2, and $ZrSiO_4$, shows spectral features different from those of metamict zircon samples. Thermal annealing of a highly damaged zircon leads to recovery of the structure of zircon, indicated by spectral changes of multi-phonon bands and U ions, accompanied with the appearance of new OH species. The results confirm that the recrystallization process in heavily damaged zircon involves the decomposition of metamict $ZrSiO_4$ into SiO_2 and ZrO_2 near 1100 K and the significant crystal growth of $ZrSiO_4$ near 1400 K as indicated by the recovery of Si–O stretching overtones and U^{4+} and U^{5+} bands.

[3] Author to whom any correspondence should be addressed.

0953-8984/02/123333+20$30.00

1. Introduction

Zircon ($ZrSiO_4$) is tetragonal with space group D_{4h}^{19} or $I4_1/amd$ and $Z = 4$ (Hazen and Finger 1979). It has been proposed as a candidate for use in the immobilization and disposal of high-actinide nuclear wastes and weapons-grade Pu. Natural zircon ($ZrSiO_4$) commonly contains U, Th, and other rare-earth elements. Due to radioactive decay of naturally occurring radionuclides and their daughter products in the ^{238}U, ^{235}U, and ^{232}Th decay series, natural minerals can be heavily damaged over geological times, resulting in an aperiodic or amorphous state—the metamict state (Ewing 1994, Salje *et al* 1999). Extensive investigations were carried out in order to gain a better understanding of the damage mechanism of zircon (Holland and Gottfried 1955, Murakami *et al* 1991, Woodhead *et al* 1991a, Farges 1994, Weber *et al* 1994, Meldrum *et al* 1998, Salje *et al* 1999, Ríos *et al* 2000, Zhang *et al* 2000c, Zhang and Salje 2001), the structural state of the amorphized phase (Farnan and Salje 2001, Trachenko *et al* 2001, Zhang and Salje 2001), and the recrystallization path (Weber 1991, Ellsworth *et al* 1994, Colombo *et al* 1999, Zhang *et al* 2000a, 2000b, Geisler *et al* 2001).

As a part of our recent systematic study of metamictization and recrystallization of zircon using Raman and infrared (IR) spectroscopy (e.g., Raman studies by Zhang *et al* (2000a, 2000c); and mid-infrared (MIR) and far-infrared (FIR) studies by Zhang *et al* (2000b) and Zhang and Salje (2001)), we undertook this near-infrared (NIR) study to gain further understanding of the damage and recrystallization processes in metamict zircon. Our principal objectives were as follows.

(1) It was reported that in the Si–O overtone region, spectral features of metamict zircon appeared similar to those of SiO_2 glass, although neither SiO_2 nor ZrO_2 were detected in metamict zircons (Vance 1975). Furthermore, IR data from the fundamental Si–O stretching bands between 800 and 1200 cm^{-1} showed spectral features very different from those of SiO_2 glass (Zhang *et al* 2000b, Zhang and Salje 2001). We wish to gain structural information through characteristic spectral changes related to multi-phonon processes, and to investigate the spectral similarities or differences among metamict zircon, decomposed zircon, and SiO_2 glass.

(2) In natural zircon, hydrogen has been found incorporated into the crystal structure, and U atoms can replace Zr atoms and still hold the D_{2d} site symmetry. Thus both OH and U ions exist as defects in natural zircon, and their characteristic spectral features are sensitive to the alternations of the crystal structure of zircon. We wish to understand the impact of radiation damage on crystal defects in zircon through analysing OH species and U ions, and to gain information on the structural change in metamictization from the variations of the defect spectra.

(3) IR spectroscopic studies have shown differences in thermal behaviour of the OH species between metamict zircon and metamict titanite ($CaTiSiO_5$). New OH species tend to form in metamict zircon during recrystallization at high temperatures (Woodhead *et al* 1991b), whereas annealing of metamict titanite leads to an increase in intensity from the original OH species existing in crystalline titanite (Salje *et al* 2000, Zhang *et al* 2001). We aim to gain a further understanding of the effects of radiation damage on OH species, and to explore what the possible structural changes causing these effects are.

2. Experimental details

The samples used in this study were analysed by electron microprobe, x-ray, and IR spectroscopy. They have been previously characterized (Murakami *et al* 1991, Ellsworth

et al 1994, Ríos and Salje 1999, Salje *et al* 1999, Ríos *et al* 2000, Zhang *et al* 2000a, 2000b, 2000c, Zhang and Salje 2001). The lattice parameters of some samples were determined by x-ray Guinier powder diffraction with Si as an internal standard. Electron microprobe analysis was performed on polished thin sections of zircon samples using a Cameca SX5D electron microprobe with a Link AN10000 energy-dispersive spectrometer. A beam size of 5 mm was used with a beam current of 100 nA. The samples used are mainly crystals from Sri Lanka because they were of gem quality and contained low chemical impurity levels.

Zircon crystals with gem quality or close to gem quality and with no cracks were selected. The crystallographic orientations of the crystals were determined from the external morphology or using x-ray precession techniques and an optical polarizing microscope. It was impossible to orient samples with doses higher than 10×10^{18} α-events g^{-1} as there were no Bragg reflections and these high-dose samples all had irregular external shapes. Crystal zircon plates were cut parallel to the $\boldsymbol{c}$-axis and were then polished.

High-temperature annealing experiments were carried out in N_2 atmosphere in a vertical furnace. The annealing temperature was measured with a Pt–PtRh thermocouple that was placed just above the samples. The sample was annealed at a high temperature for 1 h and then quenched in air. After experiments at room temperature, the samples were annealed at a higher temperature. A Leybold two-stage closed-cycle helium cryostat with a working temperature range of 13–310 K was used for *in situ* low-temperature measurements (Zhang *et al* 1996). The cryostat was coupled with a Leybold TLC60 temperature controller and a Leybold cryo-compress. A sample holder was made from high-thermal-conductivity oxygen-free copper. A gold-coated lattice made from oxygen-free copper was installed at the sample position to improve the thermal contact between the sample and the sample holder. One temperature sensor, positioned near the heating unit, was used to control the temperature of the cryostat while another Si-diode temperature sensor (LakeShore, DT-470-DI-13, calibrated by the manufacturer) was glued on the centre of the sample holder for measuring the sample temperature. The temperature stability is better than 0.2 K. The sample was placed in a vacuum chamber equipped with KRS5 windows.

Two IR spectrometers were used. A Bruker FT-IR 66v spectrometer was used to record the IR spectra between 500 and 11 000 cm^{-1} at room temperature. A liquid-nitrogen-cooled MCT detector, coupled with a KBr beam splitter and a Globar source, was used to record the spectra between 500 and 5000 cm^{-1}. For the frequency region of 3000–11 000 cm^{-1}, a tungsten source, an MCT detector, and a CaF_2 beam splitter were used with a spectral resolution of 4 cm^{-1}. A KRS5 wire-grid polarizer was employed. All the spectra were averaged over 512 scans. A Bruker 113v IFS FT-IR spectrometer was used to record polarized and unpolarized IR spectra between 1300 and 4500 cm^{-1} at low temperatures. An instrumental resolution of 2 cm^{-1} and 350 scans were adopted. Sample and reference single-beam spectra measured at the same temperatures were used for calculating the absorption spectra. All absorption spectra were recorded as absorbance α, with $\alpha = -\log_{10}(I_{\text{sample}}/I_{\text{reference}})$, where I is the single-beam transmission intensity. The software OPUS-IR was used for data analysis.

3. Analysis and results

3.1. Effect of radiation damage on multi-phonons

Polarized IR data between 1500 and 4000 cm^{-1} are plotted in figure 1. The IR spectra show two groups of separated spectral features, and they are located between 1500 and 2700 cm^{-1} and 3000 and 3600 cm^{-1}, respectively. The former is mainly due to multi-phonon interactions from the framework of zircon, whereas the latter can be mainly assigned as OH species (Dawson

Table 1. Multi-phonon bands of crystalline and weakly damaged zircon between 1350 and 2100 cm^{-1}. Sample dosages are in units of 10^{18} α-events g^{-1}. Some weak bands are undetectable in the sample with the dose of 1.8×10^{18} α-events g^{-1}. UD = undetectable.

	$\boldsymbol{E} \perp \boldsymbol{c}$		$\boldsymbol{E} \parallel \boldsymbol{c}$	
Sample dose	0.06	1.8	0.06	1.8
	1374	UD	1395	UD
	1388	UD	1445	UD
	1442	1440	1546	1533
	1516	1503	1594	1584
	1596	1588	1624	1613
	1624	1616	1661	1651
	1681	UD	1782	1760
	1720	UD	1838	1815
	1838	1815	1878	1878
	1873	1856	1909	UD
	1900	1893	1946	1934
	1953	1939	1991	UD
	1994	1986	2019	2001
	1986	UD	2046	2032
	2067	2052		

et al 1971, Woodhead *et al* 1991a, 1991b). The signals between 1350 and 2100 cm^{-1} (their peak positions are listed in table 1) are mainly related to two-phonon processes (first overtones and combinations) (Dawson *et al* 1971), and the absorption near 2700 cm^{-1} was assigned to the three-phonon process that was used to determine the degree of radiation damage in natural zircon by Woodhead *et al* (1991a).

The effects of radiation damage on the crystal structure of zircon are characterized by a dramatic decrease in intensity, and significant line broadening of the two-phonon-interaction bands of Si–O stretching between 1500 and 2100 cm^{-1} (figures 1, 2(*a*) and (*b*)). In particular, the frequencies related to the two-phonon interactions decrease systematically with increasing radiation dose. This observation is consistent with the observations from Raman bands of zircon (Zhang *et al* 2000c), which show a significant decrease of Si–O stretching vibrations in damaged zircon. Radiation damage of zircon is also characterized by systematic changes of the absorption coefficient of the minimum near 1670 cm^{-1} and the local maximum near 1873 cm^{-1} (the maximum, in fact, shifts to 1813 cm^{-1} for heavily damaged zircon) for $\boldsymbol{E} \perp \boldsymbol{c}$. The absorption coefficients of the signals are plotted as a function of radiation dose (figures 3(*a*), (*b*)). The data shown in figure 3(*a*) can be used to estimate the degree of damage. We were surprised to note that the dose dependence of the absorption coefficient at 1666 cm^{-1} (i.e., $\sim$6 μm) reported by Wasilewski *et al* (1973) gave much higher values of the coefficient than ours for damaged samples, especially at high doses. For example, a value of 62.9 cm^{-1} for the coefficient was reported for a sample with a radiation dose of 8.3×10^{18} α-events g^{-1}, and an error of 10% was estimated (Wasilewski *et al* 1973). Their absorption coefficient is almost double the value we obtained for a sample with a similar value of radiation dose. In order to check the accuracy of our measurements, the measured absorption coefficient of a sample with a dose value of 11.7×10^{18} α-events g^{-1}, which was previously measured by Aines and Rossman (1986) and Woodhead *et al* (1991a), was compared with the results of these two previous investigations. The coefficient from our measurement is consistent with those of Aines and Rossman (1986) and Woodhead *et al* (1991a). The difference between our measurement and those of Aines and Rossman (1986) and Woodhead *et al* (1991a) is less than

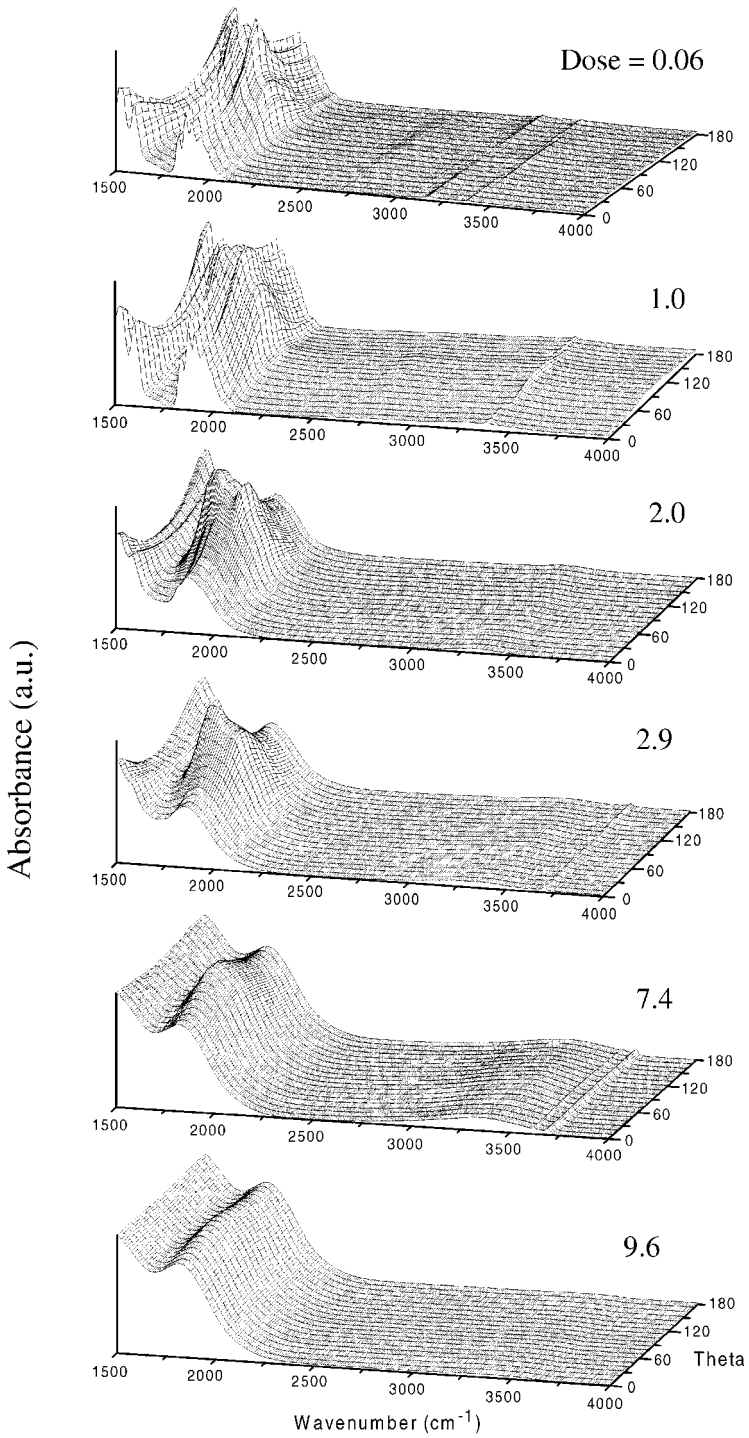

Figure 1. Polarized IR spectra between 1500 and 4000 cm^{-1} for zircon samples with different degrees of radiation damage. θ is the angle between the electric field, $\boldsymbol{E}$, and the $\boldsymbol{c}$-axis. It varies from 0 to 180°. The dose values (in units of 10^{18} α-events g^{-1}) are given in the plot. The sample with a dose value of 9.6×10^{18} α-events g^{-1} still shows a weak orientational dependence.

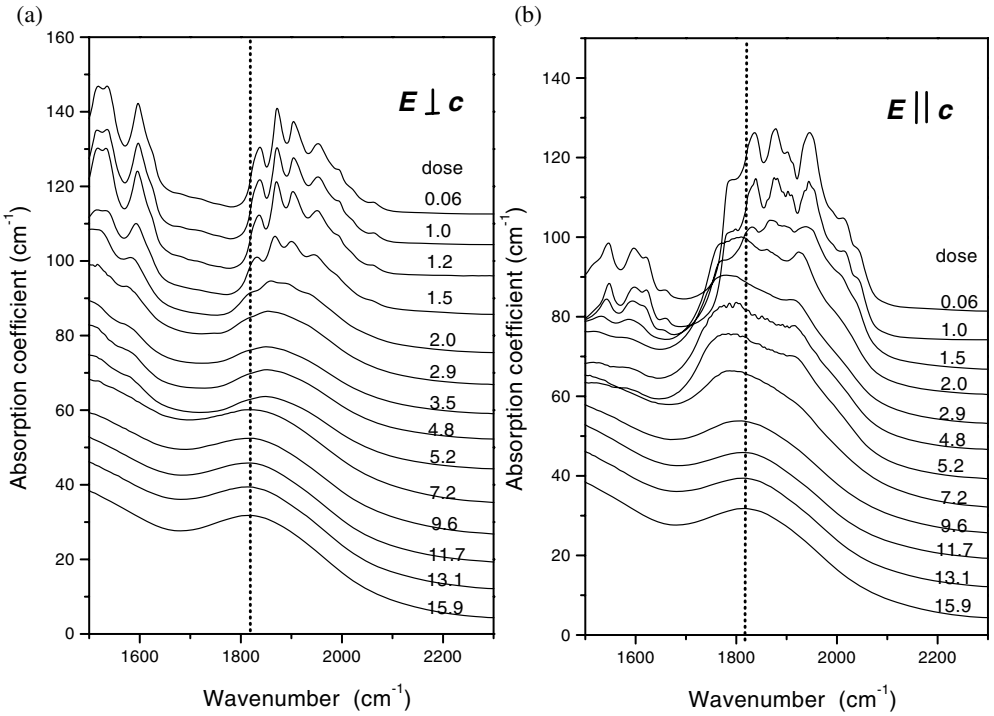

Figure 2. Effects of radiation damage on the IR bands due two-phonon interactions of Si–O stretching. The polarized spectra of samples with doses higher than 10×10^{18} α-events g^{-1} were obtained from sample plates with unknown crystallographic orientations, as they are isotropic. (*a*) $\boldsymbol{E} \perp \boldsymbol{c}$; (*b*) $\boldsymbol{E} \parallel \boldsymbol{c}$.

4%. We consider that the systematic difference between the data of Wasilewski *et al* (1973) and the three later measurements could be due to possible experimental errors. The values from Aines and Rossman (1986), Woodhead *et al* (1991a), and ours are more reliable and are fully reproducible.

The radiation-induced loss of anisotropy is shown in figure 1. The spectral features of the two-phonon bands between 1500 and 2100 cm^{-1} become more and more isotropic. However, a sample with a dose of 9.6×10^{18} α-events g^{-1} still shows a weak orientational dependence (figure 1). It is impossible to align crystallographically crystals with doses higher than 10×10^{18} α-events g^{-1} for the reasons described in the previous section. Polarized spectra measured at different polarization directions appear to show similar spectral features. This is consistent with results from polarized reflectance spectra between 650 and 1500 cm^{-1} (Zhang *et al* 2000b).

3.2. OH species

Crystalline zircon from Sri Lanka shows OH bands near 3176, 3417, and 3510 cm^{-1} for $\boldsymbol{E} \parallel \boldsymbol{c}$, 3179, 3386, and 3504 cm^{-1} for $\boldsymbol{E} \perp \boldsymbol{c}$ (figures 4(*a*) and (*b*)). The 3417 and 3386 cm^{-1} bands are associated with Si-occupied tetrahedra (Woodhead *et al* 1991b). The 3417 cm^{-1} band ($\boldsymbol{E} \parallel \boldsymbol{c}$) and the 3504 cm^{-1} band ($\boldsymbol{E} \perp \boldsymbol{c}$) have frequencies similar to those of the OH stretching band in synthetic hydroxylated zircon reported by Caruba *et al* (1985). This observation could imply the possible occurrence of the hydrogrossular substitution. As the bands are weak,

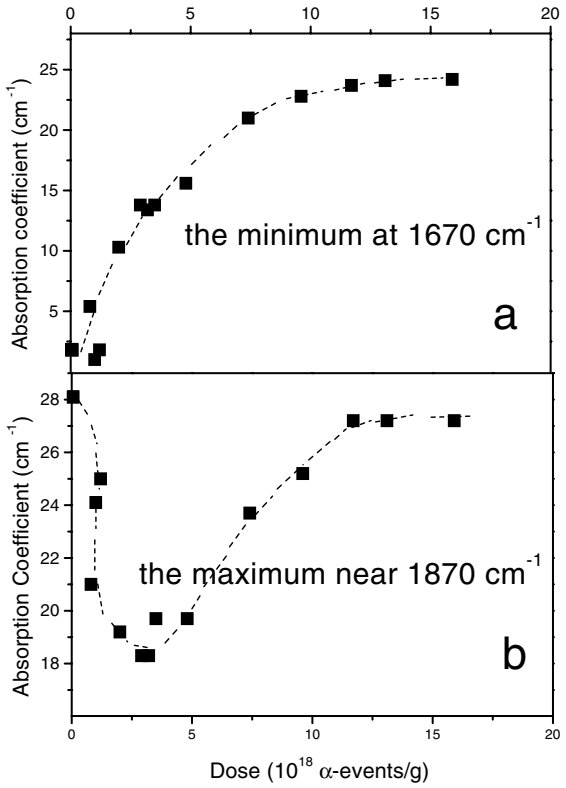

Figure 3. Dose dependences of the spectral profile with $\boldsymbol{E} \perp \boldsymbol{c}$. (*a*) The absorption coefficient of the minimum near 1670 cm^{-1}; (*b*) the absorption coefficient of the peak maximum near 1870 cm^{-1}. Dosage is in the units of 10^{18} α-events g^{-1}.

they are unlikely to play important roles in the assessment of OH contents in these samples. The effects of radiation damage on zircon are also characterized by spectral variations in OH bands (figure 1). Our results reveal that with increasing degree of damage, OH spectra exhibit the following two types of significant change. (1) The disappearance or line broadening of the sharp signals near 3179 and 3386 cm^{-1} with $\boldsymbol{E} \perp \boldsymbol{c}$ and 3417 cm^{-1} with $\boldsymbol{E} \parallel \boldsymbol{c}$, accompanied with the occurrence a broad feature in the region of 3000 and 3600 cm^{-1} at doses between 1.0 and 1.5 $\times$ 10^{18} α-events g^{-1}. (2) A systematic development of absorption signals near 3560 cm^{-1} between 4.5 and 10 $\times$ 10^{18} α-events g^{-1} as indicated by arrows (figures 4(*a*) and (*b*)). Samples with doses higher than 10 $\times$ 10^{18} α-events g^{-1} appear to show basically identical OH features. Similar spectral features were reported for highly damaged zircon by Aines and Rossman (1986) and Woodhead *et al* (1991b). We note that the effect of radiation damage on the OH species in zircon appears more complex and different from those in titanite. In titanite, the OH species eventually show a superposition of signals from crystalline and amorphous regions (Zhang *et al* 2001), but this behaviour is not observed in zircon.

Three samples (with doses of 1.5, 4.8, and 15.9 $\times$ 10^{18} α-events g^{-1}, respectively) were measured at low temperatures between 20 and 300 K in order to resolve the OH species and to identify the possible peak positions for their broad OH features (figures 5(*a*)–(*c*)). The slightly damaged sample (with a dose of 1.5 $\times$ 10^{18} α-events g^{-1}) exhibits the strongest response to

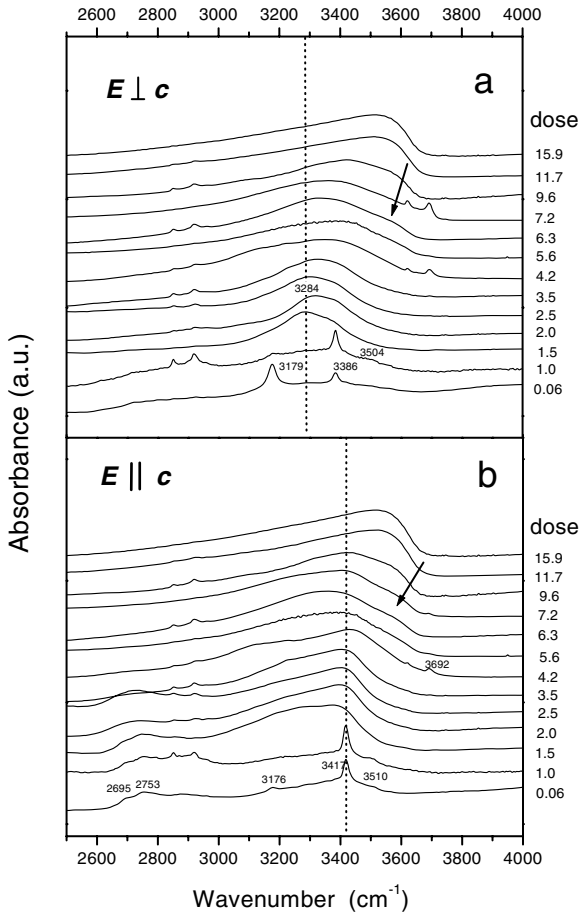

Figure 4. Infrared spectra of hydrous species for Sri Lanka zircons with different degrees of radiation damage in the region of 2500 and 4000 cm^{-1}. The spectra are normalized by height to show detailed changes. OH species show a dramatic change of the spectral patterns near 1.5×10^{18} α-event g^{-1}. Additional absorption near 3560 cm^{-1} as indicated by the arrows gradually develops between 4.5 and 10×10^{18} α-events g^{-1} and it shows a systematic increase of absorbance with increasing dose. The features near 2847 and 2817 cm^{-1} are artifacts caused by the beam splitter. (*a*) $\boldsymbol{E} \perp \boldsymbol{c}$; (*b*) $\boldsymbol{E} \parallel \boldsymbol{c}$.

decreasing temperature: the broad OH features between 3000 and 3600 cm^{-1} become sharp, showing individual peaks centred at 3298, 3336, and 3406 cm^{-1} for $\boldsymbol{E} \perp \boldsymbol{c}$, and 3183, 3280, and 3406 cm^{-1} for $\boldsymbol{E} \parallel \boldsymbol{c}$. These new OH species were not observed in samples with lower dose values, and they could result from local structural modifications in this sample. For the two more damaged samples, cooling to 20 K did not cause significant changes in peak profiles although the spectra of the samples recorded at 20 K show slightly higher integrated absorbance (2–4%) between 2500 and 3800 cm^{-1} than those measured at 300 K. This suggests that OH species of damaged samples are weakly temperature dependent. Similar observations have been made during an *in situ* IR study of metamict titanite at low temperatures (Zhang *et al* 2000d).

Due to lack of calibration between IR absorption and OH contents for zircon, we used the calibrations of Paterson (1982) to estimate the OH content in damaged zircon. This calibration

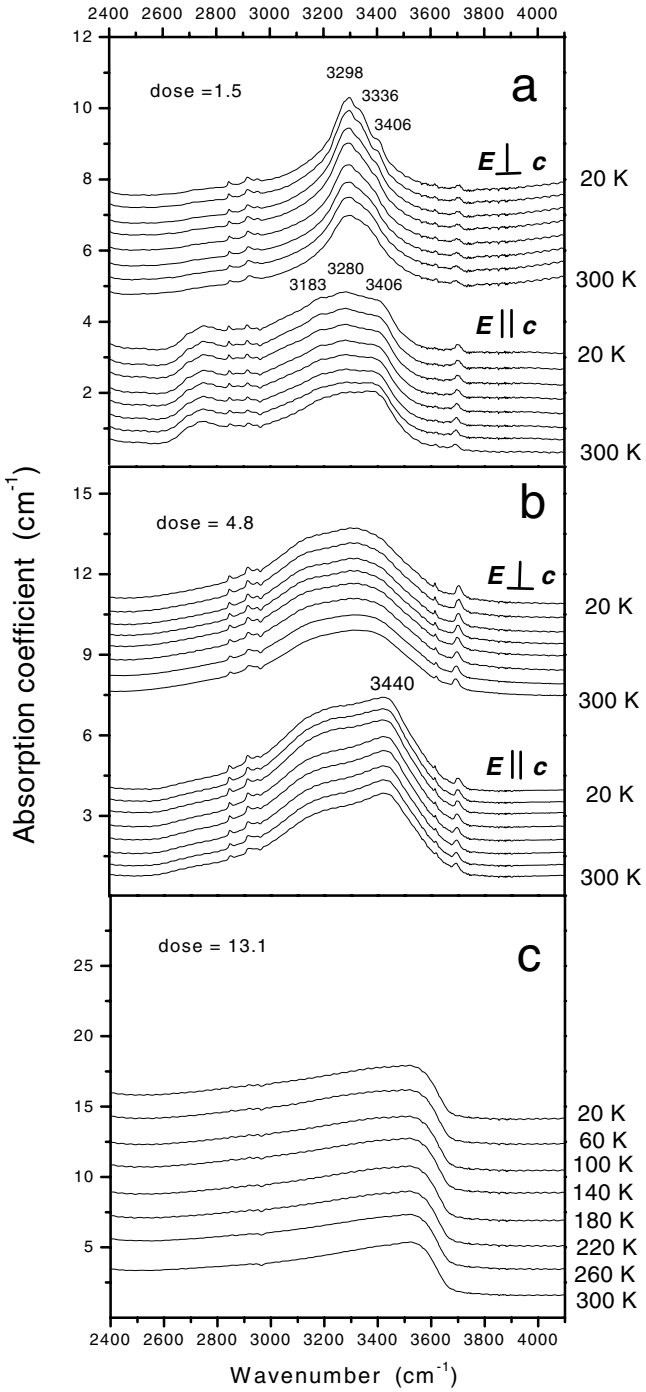

Figure 5. OH spectra of zircon with different degrees of damage between 20 and 300 K (the temperature interval = 40 K). (*a*) dose = 1.5, (*b*) 4.8, and (*c*) 13.1 × 10^{18} α-events g^{-1}. The sample with a dose of 1.5 × 10^{18} α-events g^{-1} shows relatively strong temperature responses, revealing OH bands at 3298, 3336, and 3406 cm^{-1} for $\boldsymbol{E} \perp \boldsymbol{c}$, and 3183, 3280, and 3406 cm^{-1} for $\boldsymbol{E} \parallel \boldsymbol{c}$ at 20 K. The spectra for the sample with a dose of 13.1 × 10^{18} α-events g^{-1} were obtained from sample plates with unknown crystallographic orientations because of their isotropy. The sharp weak signals near 2846, 2952, and 2917 cm^{-1} are caused absorption from the IR instruments.

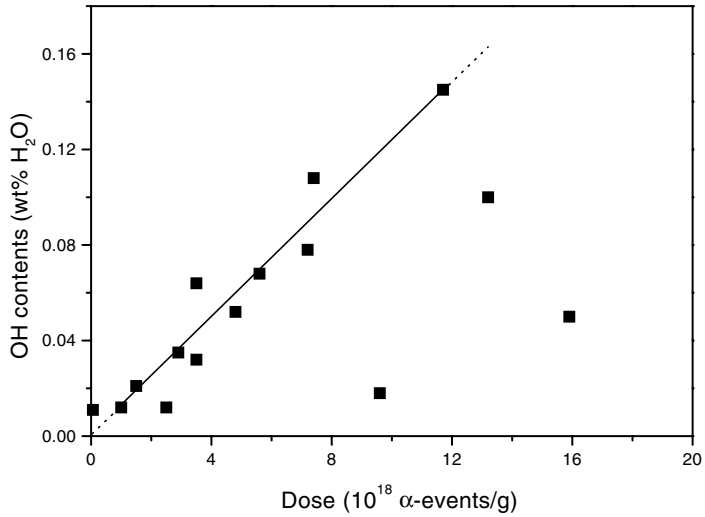

Figure 6. OH content of zircon as a function of radiation dose. The estimate of the OH concentration is obtained using the calibration of Paterson (1982) (please see the related text for details). The generally higher OH content for damaged samples shows that metamictization is one of the causes for the higher OH content in heavily damaged samples. The scattering data in the high-dose region indicate that OH is not the only parameter that affects the OH contents.

has been used to determine OH contents in metamict minerals (Woodhead *et al* 1991b, Zhang *et al* 2001). According to Paterson (1982), the OH content can be worked out using the equation:

$$c = \int \frac{K(\nu)}{150\gamma(3780 - \nu)}\,\mathrm{d}\nu \tag{1}$$

where c is the molar concentration, K the absorption coefficient, γ the orientation factor, and ν the wavenumber; $\gamma = 1/3$ was used for heavily damaged samples (dose $>10 \times 10^{18}$ α-events g^{-1}) because their spectral features are isotropic and c is in units of (mol H) L^{-1}. For crystalline and intermediately damaged zircons, $\gamma = 1/2$ and 1 were used for the spectra with $\boldsymbol{E} \perp \boldsymbol{c}$ and $\boldsymbol{E} \parallel \boldsymbol{c}$, respectively. The total content results from the sum of the two components. Since Paterson (1982) used also glasses for the calibration, the calibration diagram is considered acceptable for the estimation of water in metamict substances. In a recent paper of Libowitzky and Rossman (1997), this diagram was essentially confirmed by calibration with crystalline minerals. The estimated OH contents from our measured data are shown in figure 6.

3.3. U-ion spectra

The absorption lines of crystalline zircon between 4000 and 11 000 cm^{-1} are mainly due to U ions (figure 7(*a*)). The first overtones of the OH species and the combinations of OH stretching with the framework are expected to appear near 7200 and 4500 cm^{-1}, respectively, but they are too weak to be detected due to relatively low OH contents and small sample thickness. In crystalline zircon, the Z_r^{+4} site (with symmetry D_{2d}) can be occupied by the uranium ions. The electronic energy levels of U^{4+} and identification of the U^{4+} spectrum were obtained for U-doped synthetic zircon (Richman *et al* 1967, Vance and Mackey 1978). The U energy levels can be labelled in terms of five irreducible representations of the D_{2d} point group: four singlets Γ_1, Γ_2, Γ_3, Γ_4 and one doublet Γ_5. The degenerate $5f^2$(SL)J terms split into 70 levels:

$16\Gamma_1 + 9\Gamma_2 + 12\Gamma_3 + 12\Gamma_4 + 21\Gamma_5$, i.e., 49 singlets $\Gamma_1, \Gamma_2, \Gamma_3, \Gamma_4$ and 21 doublets Γ_5. For crystalline zircon, our data are consistent with published results (Richman *et al* 1967, Vance and Mackey 1978). Absorption lines near 6668 and 9030 cm^{-1} were observed in this study, and they were assigned as signals due to U^{5+} in optical and Zeeman studies (Vance and Mackey 1974, 1975). The presence of U^{5+} in damaged zircon is surprising, although U^{5+} has been observed in other minerals (Burns and Finch 1999). Judd and Runciman (1976) proposed that it was due to $\Gamma_6 \rightarrow \Gamma_6$ and $\Gamma_7 \rightarrow \Gamma_7$ transitions. Experimental results (Vance and Mackey 1978) confirmed the prediction and revealed that there was no accidental degeneracy in the ground state of U ions. They found that it was caused by impurity-induced new transitions rather than radiation-damage-induced signals. The observation of strong signals from these two lines in crystalline and weakly damaged zircon support the results of Vance and Mackey (1978). No evidence for the presence of U^{6+} was observed in the U-ion spectrum of zircon by Vance and Mackey (1974). The effects of radiation on the structure of zircon are characterized by three types of spectral variation.

(1) The systematic broadening of the uranium spectra (figures 7(*a*) and (*b*)) with increasing radiation dosage reflects radiation-induced damage and modifications of local structures. The linewidth for weakly damaged zircon (e.g., dose $= 1.0 \times 10^{18}$ α-events g^{-1}) is around 50 cm^{-1} for the U^{4+} signal near 4833 cm^{-1}. It becomes more than 200 cm^{-1} in samples with dose values higher than 5×10^{18} α-events g^{-1}.

(2) Dramatic intensity changes were recorded. The intensity changes in the U-ion spectrum of zircon are related to two different causes: increase of U concentration and radiation damage. These two factors have opposite effects on the intensity. In comparison with undamaged samples, the increase in intensity in weakly damaged samples is mainly due to their relatively high U concentrations. A close linear correlation between the intensity of the U^{4+} spectrum and the U concentration is observed (figure 8) and the results are consistent with the data reported by Vance and Mackey (1974), suggesting that these lines are due to U ions. The effect of radiation damage on the intensity can be seen more clearly in samples with an intermediate degree of damage, where the signals due to amorphous regions show broad features for both $\boldsymbol{E} \perp \boldsymbol{c}$ and $\boldsymbol{E} \parallel \boldsymbol{c}$, and signals related to crystalline regions still exhibit relatively sharp and anisotropic bands. With increasing degree of damage, the relative intensity of the amorphous phase increases further, whereas the signals of crystalline domains become undetectable.

(3) We noted in slightly and weakly damaged samples ($0.06–1.5 \times 10^{18}$ α-events g^{-1}) a systematic change of peak profiles occurred: the U^{5+} signal near 6668 cm^{-1} became weaker with increasing degree of damage whereas a new peak appeared near 6650 cm^{-1} (figures 7(*a*) and (*b*); the data shown in figure 7(*b*) are normalized to show the detailed changes). A similar change was also recorded for the U^{5+} line near 9030 cm^{-1} in the spectra with $\boldsymbol{E} \parallel \boldsymbol{c}$. The peak near 6650 cm^{-1} weakened in intensity with further increasing radiation dose and became unresolvable above 6×10^{18} α-events g^{-1} (figure 7(*a*)). Data from an annealed zircon (see below) show that the 6668 cm^{-1} band was recovered after high-temperature annealing. This indicates that radiation damage, instead of chemical impurities, accounts for the disappearance of the 6668 cm^{-1} line, the appearance of the 6650 cm^{-1} signal (figure 7(*b*)), and the dramatic decrease in intensity for the 6650 cm^{-1} signal in the higher-dose range.

For heavily damaged zircon, the U-ion spectra are dominated by two broad spectral features with relatively strong intensity in the regions of 4500–5500 cm^{-1} and 8400–10600 cm^{-1} (figure 7(*a*)). The former is centred near 4800 cm^{-1}, which is close to the U^{4+} band near 4833 cm^{-1}. The latter spreads over a large frequency region, and it appears to show several local

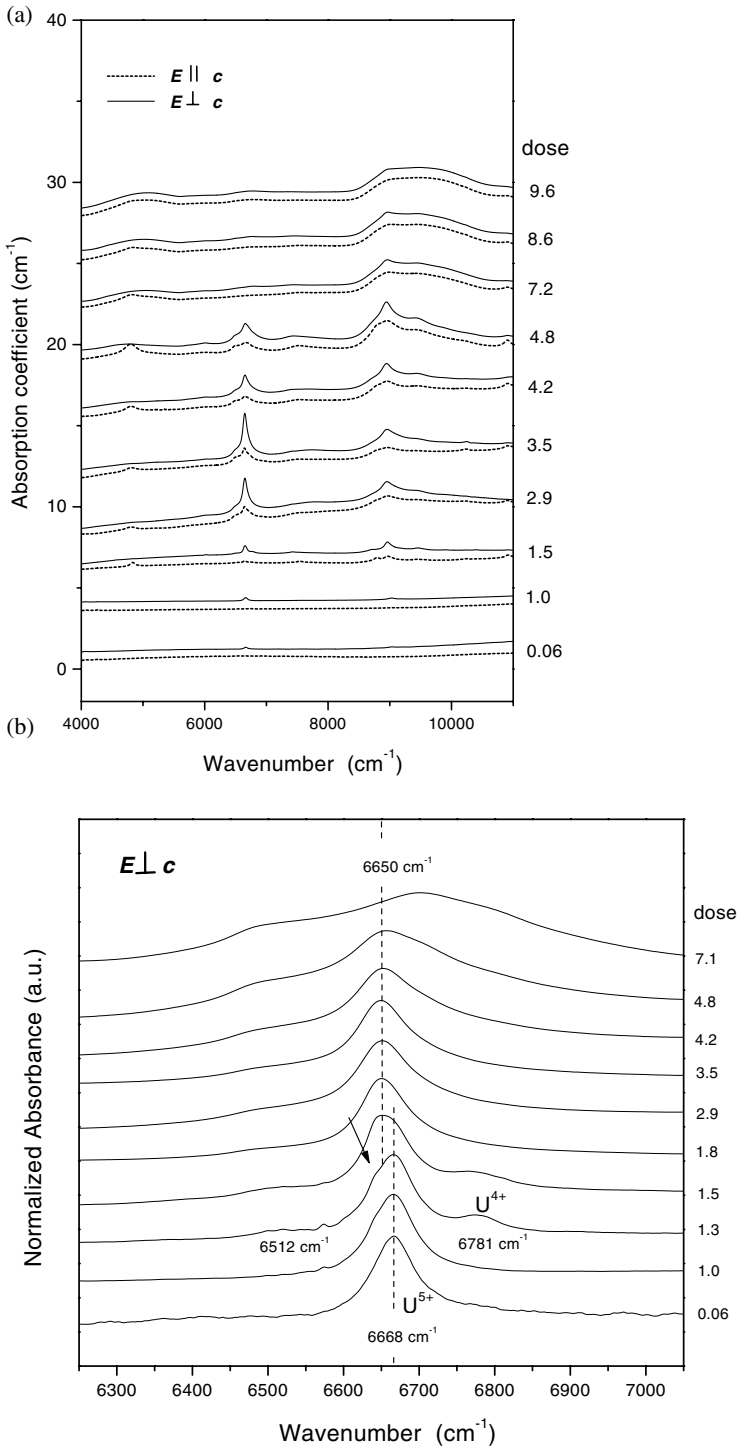

Figure 7. U-ion spectra. (*a*) Between 4000 and 11 000 cm^{-1}. The solid curves represent data with $\boldsymbol{E} \perp \boldsymbol{c}$ and the short-dashed curves those for $\boldsymbol{E} \parallel \boldsymbol{c}$. (*b*) Spectra ($\boldsymbol{E} \perp \boldsymbol{c}$) between 6200 and 7100 cm^{-1}, normalized to show detailed changes for the band near 6668 cm^{-1} and the appearance of new bands.

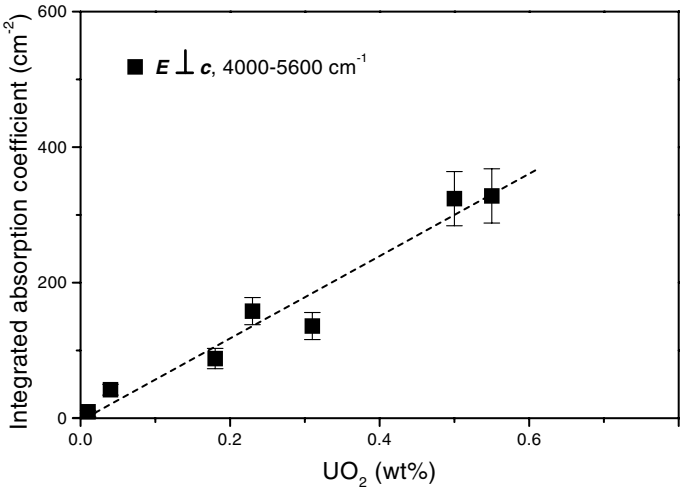

Figure 8. The integrated absorption coefficient between 4000 and 5600 cm^{-1} ($\boldsymbol{E} \perp \boldsymbol{c}$) as a function of uranium concentration. The line is a visual guide.

maxima. A weak local maximum near 6750 cm^{-1} also appears for highly damaged samples. Although it is broad and has relatively low intensity, it is resolvable (e.g., for the sample with dose $= 9.6 \times 10^{18}$ α-events g^{-1} in figure 7(*a*)). The general shape of the U-ion spectrum of the crystalline zircon is somehow still preserved for highly damaged zircon (figure 7(*a*)) although the U^{5+} signals decrease dramatically with metamictization. This observation implies that some kinds of short-range order or local order abound U ions (i.e., abound Zr sites) may still persist in the metamict state of zircon. There are significant differences between the U-ion spectra of the metamict zircon and the UO_2 (UO_2 spectrum that was reported by Griffiths and Hubbard (1991)), so the possibility of the formation of UO_2 can be ruled out.

3.4. Spectral differences between metamict and decomposed zircons

The presence of tetragonal ZrO_2 and SiO_2 glass was observed in only one natural zircon among a large number of zircon samples with a large range of radiation dose (Zhang *et al* 2000c). The sample is a green gemstone, like most heavily damaged samples analysed. However, it shows Raman signals of $ZrSiO_4$ and additional sharp Raman bands at 146, 260, 312, 460, and 642 cm^{-1} characteristic of tetragonal ZrO_2 (Zhang *et al* 2000c). X-ray diffraction data show that the sample is partially metamict. This decomposed zircon shows Si–O overtone and combination bands very different from those for the metamict zircon (figure 9). With $\boldsymbol{E} \perp \boldsymbol{c}$, it exhibits an intense Si–O stretching overtone at 1869 cm^{-1} accompanied with a shoulder near 1993 cm^{-1}. These features look more similar to those of SiO_2 glass (with bands at 1631, 1868, 1984, and 2261 cm^{-1}) than those of radiation-damaged zircon. In particular, the decomposed zircon shows an isotropic band near 2261 cm^{-1} which also appears in SiO_2 glass, but not in other zircon samples. This band is due to the overtone of the Si–O stretching near 1115 cm^{-1} in SiO_2 glass. This observation confirms that this sample contains SiO_2 glass. The anisotropic spectral features (the bands at 1513 and 1597 cm^{-1} for $\boldsymbol{E} \perp \boldsymbol{c}$, 1537, 1799, and 1933 cm^{-1} for $\boldsymbol{E} \parallel \boldsymbol{c}$) and the strong intensity for this decomposed sample indicate a significant amount of $ZrSiO_4$ phase, consistent with Raman and x-ray observations. The two bands near 3418 and 3632 cm^{-1} for $\boldsymbol{E} \parallel \boldsymbol{c}$ (figure 9) are considered to be due to OH species from the remaining

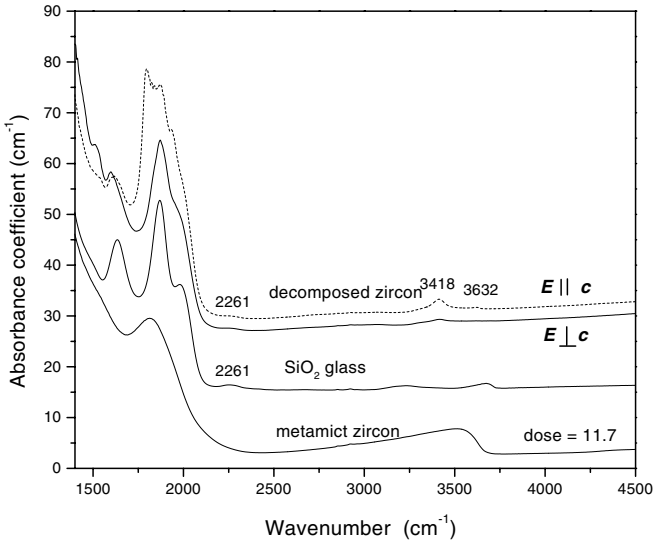

Figure 9. Spectral similarities between SiO_2 glass and decomposed zircon containing SiO_2, ZrO_2, and $ZrSiO_4$. Metamict zircon shows spectral features different from those for decomposed zircon. The spectrum of SiO_2 glass is normalized to that of the decomposed zircon to show the details. The bands near 1631, 1686, 1948, and 2261 cm^{-1} in SiO_2 glass are due to overtones and combinations of Si–O bands.

crystalline zircon in the sample because of their anisotropy. Tetragonal ZrO_2 and glassy SiO_2 phases in decomposed zircons are randomly orientated (Capitani *et al* 2000). Due to a lack of information about the thermal history of the sample, it is difficult to rule out the possibility that the presence of ZrO_2 and SiO_2 is due to its previously undergoing a high-temperature condition. In fact, this decomposed sample shows spectra with very similar features to those of a thermally treated metamict zircon in which SiO_2 and ZrO_2 were seen (see a later section). The OH spectrum of this decomposed sample exhibits only two relatively sharp bands near 3422 and 3615 cm^{-1}, in contrast to OH spectra of other zircon samples. This difference could be mainly due to the structural differences between this decomposed zircon and the metamict zircon. Our results also show clearly that the characteristic Si–O multi-phonon spectrum of highly damaged zircon is very different from that of SiO_2 glass, suggesting that Si does not exist as SiO_2 glass in the metamict state of zircon, and supporting previous IR and Raman observations of Zhang *et al* (2000b, 2000c). In contrast to the well-resolved Si–O signals in SiO_2 glass (figure 9), metamict zircon shows a broad feature with a local maximum near 1818 cm^{-1}. This implies a much more complex local configuration of SiO_4 tetrahedra in metamict zircon than that of SiO_2 glass.

3.5. Thermal annealing

A zircon crystal from Sri Lanka (with a dose of 15.9×10^{18} α-events g^{-1}) was annealed in time steps of 1 h at different temperatures in a N_2 atmosphere. The IR reflectance data on Si–O bands (650–1400 cm^{-1}, room temperature–1800 K) of this annealed crystal were published previously (Zhang *et al* 2000b). For the reasons explained in the experimental section, it was impossible to orient this high-dose sample crystallographically, and only unpolarized spectra were recorded. The two-phonon spectra (1400–2500 cm^{-1}) of the annealed sample are shown in figure 10(*a*). No significant spectral variations were seen at temperatures below 1000 K.

A broad shoulder near 1948 cm^{-1} appears near 1100 K. This feature becomes more visible in the 1200 K spectrum, and the spectral shape (figure 10(*a*)) looks similar to that of the decomposed sample in figure 9. This observation indicates that the appearance of SiO_2 glass resulted from the partial decomposition of metamict $ZrSiO_4$. The Raman spectrum of this sample annealed at 1100 and 1200 K also shows the presence of tetragonal ZrO_2. The spectra at 1400 and 1500 K show the broad characteristic signals of crystalline $ZrSiO_4$ near 1515, 1592, 1595, 1836, 1871, 1903, 1950, 1992, 2018 and 2061 cm^{-1} (obtained using the secondary-derivative method), suggesting significant crystal growth of $ZrSiO_4$. Further increasing the temperature leads to a sharpening of these lines and an increase in their intensity. The unpolarized spectra of this sample between 1600 and 1800 K, in fact, look more like the polarized spectra of crystalline samples with $\boldsymbol{E} \perp \boldsymbol{c}$ shown in figure 2(*a*). In the case of unpolarized incident radiation, the spectral feature of the sample annealed at 1800 K can only be obtained when the sample is like a 'single crystal' and its $\boldsymbol{c}$-axis is approximately parallel to the incident beam. This implies that the sample is somewhat anisotropic instead of polycrystalline. A polycrystalline sample should show IR spectra with principal components with $\boldsymbol{E} \parallel \boldsymbol{c}$ and $\boldsymbol{E} \perp \boldsymbol{c}$. X-ray measurements of the sample crystal annealed at 1800 K showed diffraction spots rather than powder rings, suggesting that it is not a polycrystal, but a crystal containing mainly a number of big 'domains' or sub-crystals with closely aligned crystallographic orientations.

The recrystallization in damaged zircon is also revealed by systematic changes in U^{4+} and U^{5+} spectra (figure 10(*b*)). The relative integrated absorbance (the integrated absorbance value of the untreated sample was set as zero) between 6200–7000 cm^{-1} was calculated to show the effect of annealing temperature (figure 10(*c*)). This frequency range was chosen, because radiation damage causes the bands near 6650 cm^{-1} to become very broad and almost undetectable in high-dose cases (figures 7(*a*) and (*b*)). The integration shows a weak increase starting near 1100 K. This is due to the appearance of weak signals of crystalline $ZrSiO_4$ as observed by Raman spectroscopy. Above 1100 K, UO_2 could also exist, because SiO_2 and ZrO_2 were observed in this annealed sample by Raman spectroscopy. However, the volume of the possible UO_2 phase must be very small because we did not detect the characteristic signals of UO_2 reported by Griffiths and Hubbard (1991). The dramatic increase of U ions signals occurred near 1400 K (figure 10(*c*)) and this indicates that the growth of $ZrSiO_4$ resulted from reaction of ZrO_2 and SiO_2 as reported previously in Raman IR studies (Zhang *et al* 2000a, 2000b).

4. Discussion

Our IR results show clearly that the contents of hydrous species in zircon are affected by metamictization. This is consistent with the observation of Woodhead *et al* (1991b). As shown in figure 6, the damaged samples tend to contain higher OH concentrations, but we also note that not all the data points fall on a line, especially for some highly damaged samples. The results imply that although the metamictization in zircon tends to result in higher OH contents, OH species are not necessarily required in the metamict state of zircon, i.e., they do not act to stabilize the metamict state. Our results also indicate that the degree of radiation damage may not be the only parameter affecting the OH content. It is likely that metamictization leads to additional sites for OH species, while the total OH contents may also be affected by other factors (e.g., geological environments and thermal history).

By comparing the OH species in metamict titanite ($CaTiSiO_5$) (Zhang *et al* 2000d), we note that OH species in metamict titanite and zircon show different responses to radiation damage. In titanite, crystalline regions show anisotropic OH absorption signals near 3486 cm^{-1} that are due to OH stretching at the O(1) site and exhibit an absorption maximum when $\boldsymbol{E}$ is approximately

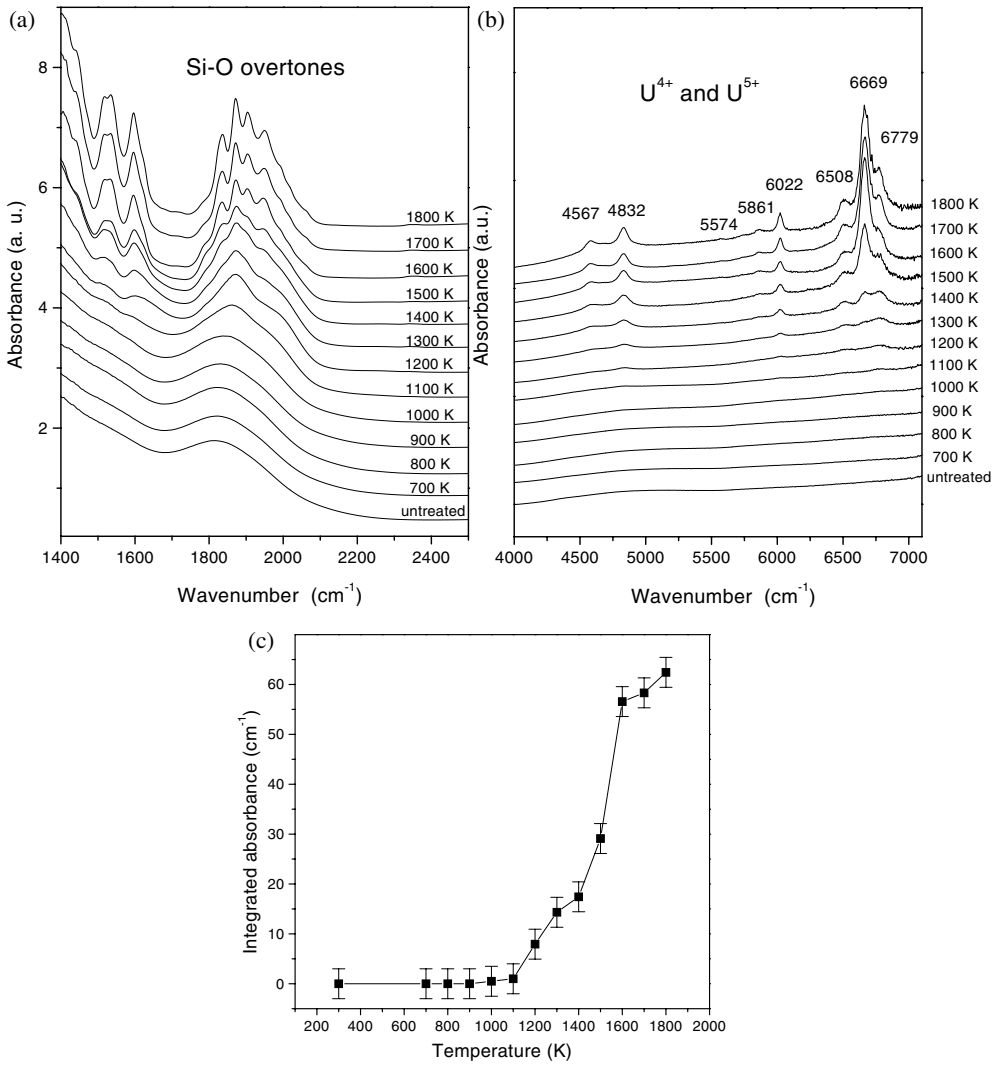

Figure 10. The effects of thermal annealing between room temperature and 1800 K on a zircon crystal with a dose of 15.9×10^{18} α-events g^{-1} and a thickness of 500 μm. (*a*) The multi-phonon spectrum between 1400 and 2500 cm^{-1}. The spectral changes near 1985 cm^{-1} taking place between 1100 and 1200 K are due to the occurrence of the thermally induced decomposition of $ZrSiO_4$ into SiO_2 and tetragonal ZrO_2 as seen by Raman investigation (Zhang *et al* 2000a) and IR reflectance measurement (Zhang *et al* 2000b). (*b*) U^{4+} and U^{5+} spectra between 4000 and 7100 cm^{-1}. The spectra were recorded using a Globar source, a KBr beam splitter, and an MCT detector. (*c*) The integrated absorbance for the features between 6200 and 7000 cm^{-1} as a function of annealing temperature.

parallel to n_α (Isetti and Penco 1968, Beran 1970), whereas metamictization produces isotropic OH features (Salje *et al* 2000, Zhang *et al* 2001). With increasing degree of damage, the OH spectra are seen as a superposition of the isotropic and anisotropic signals. In contrast, new anisotropic OH species appear in zircon with intermediate degrees of damage. They coexist with signals from the amorphized phase. As a result, the broad spectral features between 2500 and 3500 cm^{-1} in these zircon samples are still weakly anisotropic. The significant spectral

changes in the dose range of 1.0–1.5 $\times$ 10^{18} α-events g^{-1} (figure 4) may result from the formation of new OH sites in crystalline domains and the appearance of the new OH species related to the formation of amorphized phase. The signals near 3183, 3280, and 3406 cm^{-1} for $\boldsymbol{E} \parallel \boldsymbol{c}$, and 3298, 3336, and 3406 cm^{-1} for $\boldsymbol{E} \perp \boldsymbol{c}$ for a weakly damaged sample (with a dose of 1.5 $\times$ 10^{18} α-events g^{-1} shown in figure 5(*a*)) must be related to the distorted crystalline materials, for they are relatively sharp and show clearly spectral anisotropy. The contribution from the OH species related to the amorphized parts is expected to show broad and isotropic spectral features, and they are unlikely to be the principal components in this sample as its main spectral features are very different from those of heavily damaged samples. At this stage, it is impossible to access any potential influence of chemical impurities on the OH species of zircon, unfortunately. Their roles can be complex and they are beyond the scope of this study. In a recent study of OH species in titanite (Zhang *et al* 2001), the OH contents in the crystalline domains and the amorphized phase could be estimated because the OH spectra are essentially the superpositions of the two contributions. In contrast, for the case of zircon, it is impossible or difficult to estimate the portions of OH contents in the different regions. The problem, which prevents us from analysing the data further, is how to distinguish the contribution of OH species in the crystalline domains from those in the amorphized regions. We consider that the formation of the new anisotropic OH species in the samples with intermediate degrees of damage is the main cause for the different thermal behaviour of OH species observed at high temperatures in metamict zircon (Woodhead *et al* 1991b) and titanite (Zhang *et al* 2001).

One of the important questions related to the metamictization of zircon is why the moderately damaged samples generally show some characteristic signals (e.g. in x-ray diffraction, vibration modes, OH and U ions) which are absent for undamaged and highly damaged zircon samples. These signals appear related to a crystalline phase as they relatively sharp. In an x-ray and optical investigation (Holland and Gottfried 1955), it was observed that a systematic development and disappearance of an extra peak near 2θ of 35°–36.5° occurred with increasing degree of α-decay radiation damage. The authors found no appreciable variability that could be related to inhomogeneity, and proposed the formation of an intermediate polycrystalline phase with an intermediate dose. In an IR spectroscopic study (Zhang and Salje 2001), an extra absorption peak near 796 cm^{-1} was observed in moderately damaged zircon samples. This IR signal did not appear in well-crystallized samples (e.g. samples with doses $<1.5\times10^{18}$ α-events g^{-1}), but it was detected in all samples with intermediate degrees of damage. For samples with doses between 1.5 and 6.5 (in units of 10^{18} α-events g^{-1}), this peak appeared to have similar values of intensity. With further increasing dose, this peak becomes weaker, and is eventually undetectable for the heavily damaged samples (e.g., samples with doses of 9.6 and 23.5 $\times$ 10^{18} α-events g^{-1}). This peak has appeared in some IR spectra reported previously (e.g., Vance (1975), Woodhead *et al* (1991a)) although it did not seem to have drawn the attention of some authors. It was also observed in reflection spectra of moderately damaged zircon annealed at high temperatures (Zhang *et al* 2000b). According to theoretical and experimental work (Dawson *et al* 1971), $ZrSiO_4$ structure does not have an IR band near 796 cm^{-1}. In OH spectra, the spectra of zircon with intermediate degrees of damage show characteristic patterns, which are very different from those of lower- or high-dose regions. What is more, the line near 6667 cm^{-1} in the U-ion spectrum shows anomalous changes near doses of 1.5 $\times$ 10^{18} α-events g^{-1} (i.e., the appearance of an extra signal near 6650 cm^{-1}) (figure 7(*b*)). Eventually, the 6650 cm^{-1} line becomes undetectable in the spectrum of a sample with a dose of 7.1 $\times$ 10^{18} α-events g^{-1} (figure 7(*b*)). We believe that these anomalies detected by different analytic methods do not appear accidentally in the moderately damaged samples. They reflect the radiation-induced damage in crystalline regions which are 'seen' by vibrational phonons, OH species, and U ions.

OH and U ions are defects in the structure of $ZrSiO_4$. Their peak profiles (number of bands, peak positions, and shapes) are very sensitive to their local surroundings. They can be affected by the structural modification surrounding oxygen atoms. The modification may be also correlated with observed changes in cell parameters (Holland and Gottfried 1955, Murakami *et al* 1991) and vibrational bands (Zhang *et al* 2000c, Zhang and Salje 2001) in this dose range. These changes appear to suggest the existence of an intermediate state with a modified local symmetry in the moderately damaged zircon samples. We consider that chemical impurities may not be the principal cause of the spectral changes for the following reasons. Firstly, the Sri Lanka zircon samples have relatively low concentrations of chemical impurities (for information on the chemical compositions of the samples, see Zhang *et al* (2000a, 2000c)) in comparison with zircon from other localities, although one cannot rule out the possible effects of chemical impurities on OH spectra. In addition, the OH spectral features show systematic variations outside the range of 1.0–10 $\times$ 10^{18} α-events g^{-1} (figures 4(*a*) and (*b*)) which cannot be explained by chemical impurities. Furthermore, the spectral changes can be recovered through high-temperature annealing, suggesting that they are due to radiation damage.

Another possible cause for the change in U and OH spectra is radiation-induced ionization. During radioactive decays (i.e., α-, β-, and γ-decays), ionization may take place and cause variations of the charge state of lattice defects. These changes may play a significant role in the microstructural evolution of irradiated materials and result in changes in other physical properties. As a result, the mobility of the defects may be affected (Bourgoin and Corbett 1978), and eventually the chemical durability and dissolubility may be altered. The radiation-induced reduction of Fe^{3+} to Fe^{2+} was reported in metamict titanite by Hawthorne *et al* (1991). Our results suggest that U^{4+} is still the principal oxidization state of U in highly metamict zircon, although the data cannot completely rule out the possible presence of U^{6+} caused by metamictization of zircon. The presence of U^{4+} due to the daughter product of ^{238}Pu decay was recorded in Pu-doped zircon using x-ray absorption fine-structure spectroscopy at the U L_{III} edge (Hess *et al* 1998). The dramatic variations of intensity with increasing radiation dose shown by the U^{5+} bands near 6668 and 9030 cm^{-1} (figure 7(*a*)) are puzzling. Further investigations are desirable to check the physical origins.

The systematic development of the signal near 3560 cm^{-1} (figures 4(*a*) and (*b*)) in the dose range of 4–10 $\times$ 10^{18} α-events g^{-1} is surprising. This feature should be related to the amorphized phase, for it is isotropic (appearing when $\boldsymbol{E} \parallel \boldsymbol{c}$ and $\boldsymbol{E} \perp \boldsymbol{c}$ and for other orientations) and its intensity increases with increasing dose. Only very limited crystalline domains may remain in the high-dose case. Why zircon samples with such high doses show this OH feature is unclear. It is certainly related to new OH sites in these samples. It may suggest that the local configuration of the amorphized phase in the low-dose case could be modified with further damage. The development of this feature at high doses and the significant spectral change near 1.5 $\times$ 10^{18} α-events g^{-1} (figures 4(*a*) and (*b*)) could also be related to the two percolation points discussed by Salje *et al* (1999).

Our study revealed that the absorption coefficient related to the maximum near 1875 cm^{-1} (the maximum shifts to near 1815 cm^{-1} in highly damaged samples) shows a dramatic decrease up to dose of 3.5 $\times$ 10^{18} α-events g^{-1} and a systematic increase at higher dose values with increasing damage. As explained in earlier texts, the signals in this region are mainly associated with the two-phonon interactions of Si–O stretching. The observed change in fact reflects the decrease of crystalline phase fraction and the increase of amorphized phase fraction with increasing dose. Although the signal reaches its minimum near 3.5 $\times$ 10^{18} α-events g^{-1}, this does not mean that above this dose value zircon becomes fully metamict, because further spectral changes still take place at much higher doses (figures 1, 2(*a*) and (*b*)). In fact, x-ray diffraction, IR, and Raman measurements (Salje *et al* 1999, Zhang *et al* 2000b, 2000c, Zhang

and Salje 2001), for the same samples, showed that crystalline domains of $ZrSiO_4$ remained detectable even in samples with much higher dose values. In fact, as shown by Salje *et al* (1999), the fully metamict state can hardly be reached. We also note that the bands near 2700 cm^{-1}, which are mainly due to second-overtone of Si–O stretching, become undetectable when the dose is higher than 3.5×10^{18} α-events g^{-1} as reported by Woodhead *et al* (1991a). This could be due to their relatively low intensity and overlap with OH species. By comparison with the first overtones of Si–O stretching near 1700–1800 cm^{-1}, the bands near 2700 cm^{-1} are not ideal bands for the determination of the degree of damage in highly metamict zircon.

5. Conclusions

Near-IR spectroscopy has been used to investigate the metamictization process and the metamict state in zircon. The results from this study show that the effects of radiation on the crystal structure of zircon are characterized by a dramatic variation of intensity, a decrease in frequencies in multi-phonon bands, a change of spectral profile of OH species, a formation of new OH species, and new signals related to U ions. The data from moderately damaged zircon show the presence of new anisotropic OH species, implying radiation-induced new OH sites and structural modifications in the crystalline region of partially damaged zircon. The damaged zircons tend to contain higher OH concentrations. The results suggest that although the metamictization in zircon tends to result in higher OH contents, OH species are not necessarily required in the metamict state of zircon, i.e., they do not act to stabilize the metamict state. Our results also indicate that the degree of radiation damage may not be the only parameter affecting the OH content. Radiation damage causes dramatic changes in the U^{4+} and U^{5+} spectra of zircon. Our results show, for the first time, that radiation leads to the disappearance of the U^{5+} bands near 6668 and 9030 cm^{-1} and the occurrence of extra lines near 6650 and 8969 cm^{-1} at doses of around 1.5×10^{18} α-events g^{-1}. The general shape of the U-ion spectrum of the crystalline zircon is somehow still preserved for highly damaged zircon. There are significant differences between the U-ion spectra of the metamict zircon and those of UO_2. Different spectral patterns were observed for metamict zircon and a decomposed zircon. The spectrum of the decomposed sample exhibits characterized signals of SiO_2 glass in the Si–O overtone region. Thermal annealing of highly metamict zircon at high temperatures results in decomposition into SiO_2 and ZrO_2 near 1100 K. The recovery of Si–O stretching overtones and U^{4+} and U^{5+} bands near 1400 K indicates significant crystal growth of $ZrSiO_4$.

Acknowledgments

The authors are indebted to the Sedgwick Museum of the University of Cambridge, UK; the Natural History Museum, London, UK; and the Mineralogisches Museum of Universität Hamburg, Germany for providing some of the samples used in this study. Thanks are due to William Lee for reading the original manuscript.

References

Aines R D and Rossman G R 1986 *Am. Mineral.* **71** 1186
Beran A 1970 *Tschermaks Mineral. Petrograph. Mitteil.* **14** 1
Bourgoin J C and Corbett J W 1978 *Radiat. Eff.* **36** 157
Burns P C and Finch R J 1999 *Am. Mineral.* **84** 1456
Capitani G C, Leroux H, Doukhan J C, Ríos S, Zhang M and Salje E K H 2000 *Phys. Chem. Minerals* **27** 545
Caruba R, Baumer A, Ganteaume M and Iacconi P 1985 *Am. Mineral.* **70** 1224

Colombo M, Crosch J and Salje E K H 1999 *J. Am. Ceram. Soc.* **82** 2711
Dawson P, Hargreave M M and Wilkinson G F 1971 *J. Phys. C: Solid State Phys.* **4** 240
Ellsworth S, Navrotsky A and Ewing R C 1994 *Phys. Chem. Minerals* **21** 140
Ewing R C 1994 *Nucl. Instrum. Methods* B **91** 22
Farges F 1994 *Phys. Chem. Miner.* **20** 504
Farnan I and Salje E K H 2001 *J. Appl. Phys.* **89** 2084
Geisler T, Pidgeon R T, van Bronswijk W and Pleysier R 2001 *Eur. J. Mineral.* **13** 1163
Griffiths T R and Hubbard H V S 1991 *J. Nucl. Mater.* **185** 243
Hawthorne F C *et al* 1991 *Am. Mineral.* **76** 370
Hazen R M and Finger L W 1979 *Am. Mineral.* **64** 157
Hess H J, Weber W J and Conradson S D 1998 *J. Nucl. Mater.* **254** 175
Holland H D and Gottfried D 1955 *Acta Crystallogr.* **8** 291
Isetti G and Penco A M 1968 *Mineral. Petrograph. Acta* **14** 115
Judd B R and Runciman W A 1976 *Proc. R. Soc.* A **352** 91
Libowitzky E and Rossman G R 1997 *Am. Mineral.* **82** 1111
Meldrum A, Zinkle S J, Boatner L A and Ewing R C 1998 *Nature* **395** 56
Murakami T, Chakoumakos B C, Ewing R C, Lumpkin G R and Weber W J 1991 *Am. Mineral.* **76** 1510
Paterson M S 1982 *Bull. Minéral.* **105** 20
Richman I, Kisliuk P and Wong E Y 1967 *Phys. Rev.* **155** 262
Ríos S and Salje E K H 1999 *J. Phys.: Condens. Matter* **11** 8947
Ríos S, Salje E K H, Zhang M and Ewing R C 2000 *J. Phys.: Condens. Matter* **12** 2401
Salje E K H, Chrosch J and Ewing R C 1999 *Am. Mineral.* **84** 1107
Salje E K H, Zhang M and Groat L A 2000 *Phase Transitions* **71** 173
Trachenko K O, Dove M T and Salje E K H 2001 *J. Phys.: Condens. Matter* **13** 1947
Vance E R 1975 *Radiat. Eff.* **24** 1
Vance E R and Mackey D J 1974 *J. Phys. C: Solid State Phys.* **7** 1898
Vance E R and Mackey D J 1975 *J. Phys. C: Solid State Phys.* **8** 3439
Vance E R and Mackey D J 1978 *Phys. Rev.* **18** 185
Wasilewski P J, Senftle F E, Vaz J E, Thorpe A N and Alexander C C 1973 *Radiat. Eff.* **17** 191
Weber W J 1991 *Radiat. Eff. Defects Solids* **115** 341
Weber W J, Ewing R C and Wang L M 1994 *J. Mater. Res.* **9** 688
Woodhead J A, Rossman G R and Silver L T 1991a *Am. Mineral.* **76** 74
Woodhead J A, Rossman G R and Thomas A P 1991b *Am. Mineral.* **76** 1533
Zhang M, Lee G A, Salje E K H and Beran A 2001 *Am. Mineral.* **86** 904
Zhang M and Salje E K H 2001 *J. Phys.: Condens. Matter* **13** 3057
Zhang M, Salje E K H, Capitani G C, Leroux H, Clark A M and Schlüter J 2000a *J. Phys.: Condens. Matter* **12** 3131
Zhang M, Salje E K H, Ewing R C, Farnan I, Ríos S, Schlüter J and Leggo P 2000b *J. Phys.: Condens. Matter* **12** 5189
Zhang M, Salje E K H, Farnan I, Graeme-Barber A, Daniel P, Ewing R C, Clark A M and Leroux H 2000c *J. Phys.: Condens. Matter* **12** 1915
Zhang M, Salje E K H, Malcherek T, Bismayer U and Groat L A 2000d *Can. Mineral.* **38** 119
Zhang M, Wruck B, Graeme-Barber A, Salje E K H and Carpenter M A 1996 *Am. Mineral.* **81** 92